Systematic control of spectral hole burning and homogeneous linewidth by disorder in Y_2O_3:Pr^{3+} crystalline systems

Tsuyoshi Okuno* and Tohru Suemoto
The Institute for Solid State Physics, University of Tokyo, Roppongi 7-22-1, Minato-ku, Tokyo 106-8666, Japan
(Received 6 August 1998; revised manuscript received 5 October 1998)

We investigated the hole-burning phenomena and homogeneous linewidth in Pr^{3+}-doped Y_2O_3-based crystals under the systematic control of disorder in the crystal. When divalent ions are doped into an Y_2O_3:Pr^{3+} crystal, holes due to rearrangement of local structure around Pr^{3+} ions are burned. The burning curves are successfully analyzed in terms of a distributed tunneling rate model for hole formation. The burning efficiency from this analysis and the homogeneous linewidth become larger as the crystal includes a larger amount of divalent ions. The interaction of Pr^{3+} ions with oxygen vacancies is thought to be one of the origins of the hole production and the line broadening. The interaction length between Pr^{3+} ions and oxygen vacancies is discussed. [S0163-1829(99)01214-X]

I. INTRODUCTION

There are still many unsolved problems in disordered materials. For example, various aspects of their thermodynamical properties at low temperatures have been explained in terms of two-level systems (TLS), but the origin of the TLS often remains unclear.[1–3] One of the reasons for this situation is the lack of knowledge about the nature of disorder and of an experimental method to investigate it. Recently, persistent spectral hole burning has been recognized as a possible powerful tool to investigate these problems from microscopic viewpoint. This phenomenon has been extensively studied in various materials, mainly due to the possibility of its application to high-density optical memories using frequency domain recording.[4] Realization of room-temperature hole burning is one of the most attractive targets for recent research work.[5–7] On the other hand, the phenomenon of persistent hole burning is profoundly related to the nature of the disorder, and a detailed investigation of the persistent hole burning will provide a way of understanding the disordered matrix in which the optical centers are embedded.

There are several mechanisms for persistent spectral hole burning. Among them, the mechanism concerned with TLS in disordered materials is known as photophysical hole burning.[3] It is believed that some slight rearrangement of the lattice is induced by optical excitation and a spectral hole is locked persistently owing to a long recovering time of this rearranged configuration. In most cases, however, the detail of this structural change or even the relevant entity which is bringing about the TLS is not clarified. This is mainly because the investigations were done in too complicated systems such as multicomponent glasses or polymers. In order to clarify the nature or the origin of the rearrangement or the role of TLS, studies in materials with well-controlled disorder can be more fruitful approaches. Continuous changing of the degree of disorder starting from an almost perfectly ordered system will be most useful for looking at the effect of disorder in the hole properties.

In inorganic crystals or mixed crystals with simple structure suitable for the systematic control of disorder, there are only a few examples in which holes due to the lattice rearrangement have been observed. Studies on hole burning in Eu^{3+}-doped crystals were reported recently.[8,9] As for Pr^{3+}-doped crystals, it was reported that holes due to light-induced tunneling of D^- appeared in SrF_2:Pr^{3+} and CaF_2:Pr^{3+} containing D^- ions.[10,11] Holes due to the same mechanism were reported also in $SrZrO_3$:Pr^{3+} based oxides.[12] The former were reported with the interest of the holes due to optical pumping mechanism among hyperfine split levels of Pr^{3+}, and the relation between persistent holes and disorder was not discussed. Previously we reported the persistent hole in YSZ$[(ZrO_2)_{0.9}-(Y_2O_3)_{0.1}]$:$Pr^{3+}$ due to the lattice rearrangement which may be concerned with oxygen vacancies,[13,14] and also in YAG($Y_3Al_5O_{12}$, yttrium-aluminum-garnet):Pr^{3+}.[15] In addition, we reported the preliminary result that the introduction of Mg^{2+} into Y_2O_3:Pr^{3+} crystals induces persistent holes.[16,17]

As for the existence of TLS, it is more often manifested by the appearance of a nearly linear temperature dependence of the homogeneous linewidth (Γ_{hom}) at low temperatures ($\Gamma_{hom} \propto T^n$ where n is slightly greater than or equal to 1). It was shown for inorganic glasses that the same value of n observed in the hole-burning result is also found for the temperature dependence of the specific heat, consistent with theoretical models.[18]

Studies on samples with systematically controlled disorder will be also useful to understand the temperature dependence of Γ_{hom} in disordered materials. In these systems, the nature of TLS which broadens Γ_{hom} may be clarified. From the study on Γ_{hom} of Eu^{3+}:$Y_{2-x}Sc_xO_3$, it was found that disorder introduced by Sc^{3+} replacing Y^{3+} does not lead to an increase in Γ_{hom}.[19] The research in this direction should be promoted in order to understand the role and mechanisms of disorder in determining Γ_{hom} and its temperature dependence in glassy materials.

For these two purposes, that is, to clarify the hole-burning mechanism concerned with TLS and to understand the temperature dependence of Γ_{hom} in disordered materials, we applied hole-burning spectroscopy to Y_2O_3:Pr^{3+} crystals doped with various amounts of Mg ions. We also investigated

TABLE I. Samples used in this paper, including results of element analyses of metallic ions in $Y_2O_3:Pr^{3+}$ crystals, and inhomogeneous linewidths.

Sample notation[a]	Concentration of starting mixtures (mol %)		Result of element analysis of metallic element[b] (mol %)	Estimated concentration of metallic element[e] (mol %)	Inhomogeneous linewidth[f] (cm^{-1})
	Pr^{3+}	metallic element			
$Y_2O_3:Pr^{3+}$ (0.2) (undoped)	0.2				0.58±0.01
$Y_2O_3:Pr^{3+}$ (0.2)-Mg(0.1)	0.2	0.1	0.0093*	0.005±0.0025	0.64±0.01
-Mg(0.3)	0.2	0.3	0.0108	0.015±0.0075	0.66±0.01
-Mg(0.6)	0.2	0.6	(0.116)[c]	0.03±0.015	0.68±0.01
-Mg(1)	0.2	1	0.0773	0.05±0.025	0.81±0.01
-Ca(1)	0.2	1	(1)[d]		(2.4± 0.1)
-Ba(1)	0.2	1	0.0173		0.76±0.01
-Zr(5)	0.2	5	4.6*		(18± 0.1)
$Y_2O_3:Pr^{3+}$ (0.02)-Mg(0.1)	0.02	0.1	0.005 38	0.005±0.0025	

[a]Concentrations in starting mixtures (prepared batch in powder) are used for sample notations. For example, $Y_2O_3:Pr^{3+}$(0.2)-Mg(0.1) is (Y_2O_3) (99.8 mol %)-(Pr_2O_3) (0.1 mol %)-(MgO) (0.1 mol %).

[b]Results of ICP-MS (induced coupled plasma mass spectrometric analysis) or ICP (induced coupled plasma emission spectrochemical analysis, with *).

[c]This is less reliable than others, considering quality of analyzed blocks.

[d]Values larger than 1 mol % were obtained in the analysis, thus 1 mol % is assumed.

[e]Reduction factor of 1/20 from the starting mixtures and the error range of ±50% are assumed.

[f]Inhomogeneous linewidths were obtained at 4.7 K from luminescence excitation spectra, or from luminescence spectra excited nonselectively by a xenon lamp with a broad bandpass filter for the values in parentheses.

samples with some other metallic ions.

We have found in the previous paper that 20 K is most appropriate for comparing persistent holes in $Y_2O_3:Pr^{3+}$ crystals.[17,20] At temperatures higher than 20 K the hole-burning efficiency is not large due to the thermal hole-recovery process, and at lower temperatures the rearrangement mechanism is suppressed by the optical-pumping mechanism among hyperfine split levels. We first measure holes at 20 K in the five kinds of MgO-doped $Y_2O_3:Pr^{3+}$ crystals. We describe the MgO-concentration dependence of hole behavior. Then, we investigate the effect of other metallic ion doping, i.e., Ca^{2+}, Ba^{2+}, and Zr^{4+} doping. Considering these results, we discuss the origin of the lattice rearrangement. In addition, the interaction length of Pr^{3+} ions in this mechanism is estimated. Lastly, we discuss the temperature dependence of the homogeneous linewidth in the MgO-doped crystals.

II. EXPERIMENT

A. Samples

The $Y_2O_3:Pr^{3+}$ crystals were grown by the floating-zone method using a xenon arc image furnace.[21] For starting materials, powder reagents (Y_2O_3: 99.99%, Rare Metallic Co., Pr_2O_3: 99.9%, other oxides with similar grade) were used. The concentration of Pr^{3+} was always 0.2 mol % (except for one sample used in Sec. III D). We mixed the powder in the ratio of (Y_2O_3) ((99.9-x) mol %)-(Pr_2O_3)(0.1 mol %)-(metal oxide)(x mol %) and pressed it into a rod. Then, we sintered the rod around 1300 °C for a few hours in air. We grew crystals by the image furnace in an argon atmosphere with a growing velocity of ~20 mm/h.

To investigate the effect of doping divalent ions, we compare the results of doped $Y_2O_3:Pr^{3+}$ samples with that of ''undoped'' $Y_2O_3:Pr^{3+}$ used in the previous paper.[17,20] We prepared samples with four different MgO concentrations, i.e., 0.1, 0.3, 0.6, and 1 mol % in starting mixtures. In addition, samples with other divalent ions (Ca^{2+}, Ba^{2+}) and tetravalent ions (Zr^{4+}) were examined. The crystalline structures were not changed by doping of these divalent or tetravalent metallic ions in all of the $Y_2O_3:Pr^{3+}$ samples, as we confirmed it by powder x-ray-diffraction patterns.

During the crystal growing procedures, some of the divalent ions are subjected to considerable sublimation. Therefore, the real concentration of the dopant in the crystal may be different from the initial one in starting mixtures. In order to estimate the real concentrations, we made element analyses using induced-coupled plasma mass spectrometric analysis (ICP-MS) or induced-coupled plasma emission spectrochemical analysis (ICP) methods in several samples. The results are shown in Table I.

We confirmed by the ICP method that the concentration of Pr^{3+} is retained within ±30%. However, the concentration of the Mg^{2+} ions is about an order of magnitude lower than the value in the starting mixtures.[22] This is ascribed to the high volatility of MgO. It is quite difficult to estimate the real concentration of Mg^{2+} ions in the sample pieces used in the spectroscopic measurement. We have to use a different part of the block for the element analysis due to destructive nature of the ICP analysis. The rather large fluctuation in the reduction ratio of the Mg^{2+}-ion concentration may be ascribed to the inhomogeneity of the crystal blocks which were taken from the part with lower quality. The ICP results tend to be influenced by segregated Mg ions in the case of low-quality samples. For example, the relatively large value for the Mg(0.6) sample can be ascribed to this effect. The Mg^{2+}-ion concentration in the sample pieces for optical measurements is believed to be more stable. This is supported by

the smooth change of the inhomogeneous linewidth seen in Table I. The order of the concentration of Mg^{2+} among these four pieces for optical measurements is believed to be retained. As shown in Table I, the reduction factor of Mg^{2+} distributes from 1/10 to 1/27, ignoring the Mg(0.6) case. Throughout the following semiquantitative discussions, we use a reduction factor 1/20 for all the samples. The expected error range of the Mg^{2+}-concentration will be $\pm 50\%$. Table I includes the estimated concentrations of Mg^{2+}.

Considerable reduction was observed in the Ba^{2+}(1 mol %)-doped sample, while for the Zr^{4+}(5 mol %)-doped sample the initial concentration is retained after the crystallization. As for the Ca^{2+}(1 mol %)-doped sample, values larger than 1 mol % were obtained, the reason for which might be the relatively large inhomogeneity of the sample doped with Ca^{2+}. We assume 1 mol % for the concentration of Ca^{2+}. As is mentioned above, the real concentration of metallic ions are not the same as those in the starting mixtures. However, we use the concentrations in the starting mixtures for sample notations shown in Table I.

The crystal structure of cubic Y_2O_3 is of a rare-earth sesquioxide *C*-type structure with space group T_h^7 (or, $Ia3$).[23] One unit cell contains 16 Y_2O_3 molecules. There are two crystallographically different cation sites; 24 Y^{3+} ions occupy the Wyckoff position 24*d* with site symmetry C_2, and eight Y^{3+} ions occupy the position 8*b* with site symmetry C_{3i} (or, S_6). The ratio of the number of C_2 sites to that of C_{3i} sites is 3:1.

It is generally agreed that the site occupation of Pr^{3+} ions in Y_2O_3 is substitutional on the two cation sites. Absorption lines of Pr^{3+} in Y_2O_3 at 80 K were reported and assigned to the C_2 site.[24] In all of our samples, we measured luminescence and excitation spectra at 4.2 K to determine the energy separations between $^3H_4$ and $^1D_2$ levels. The energy positions of all of the absorption peaks are found to be almost exactly the same as those determined in Ref. 24; the difference is at most 6 cm^{-1}, which may be attributed to the difference of the temperature. Therefore, we conclude that Pr^{3+} ions observed by luminescence spectroscopy in our samples occupy the C_2 site where the crystalline field remains almost unchanged by the doping.

In all the samples, we measured the inhomogeneous linewidth of the $^3H_4(1)$-$^1D_2(1)$ transition (between the lowest levels of $^3H_4$ and $^1D_2$, 6189 Å) at 4.7 K. It was determined from luminescence excitation spectra for widths smaller than 1 cm^{-1}. For widths larger than 1 cm^{-1} [Y_2O_3:Pr^{3+}-Ca(1) and -Zr(5)], we used luminescence spectra excited nonselectively by a xenon lamp with a broad (~100 Å) bandpass filter around 4700 Å. The consistency between these two measurements was confirmed in Y_2O_3:Pr^{3+}-Mg(1). In Table I, we summarize the values of the inhomogeneous linewidth.

B. Hole-burning measurement

As an excitation source for hole-burning experiments, we used a single-frequency ring dye laser (Coherent CR699-21) pumped by an argon-ion laser (Spectra-physics SP2016). We made hole-burning experiments by using the $^3H_4(1)$-$^1D_2(1)$ transition of Pr^{3+} at 6189 Å. The spectral width of the dye laser due to frequency jitter is ~5 MHz (~10^{-4} cm^{-1}).

The laser beam was spatially filtered by a single-mode optical fiber. The output from the fiber was passed through a polarizer, and then stabilized by a laser power controller (CRI LPC-VIS). The laser beam was loosely focused on the sample surface with a beam diameter of 1.00 ± 0.05 mm; this diameter is retained more than 10 mm in the beam direction around sample position. This ensures the same density of the irradiating laser power on the sample, even if the sample position slightly changes. The sample surface was held at ~45° to the irradiating laser beam in a continuous-flow cryostat (Oxford CF1204).

Luminescence from the sample was collected by a lens to a photomultiplier (Hamamatsu R955) at a right angle to the laser beam. The laser light was rejected and the luminescence was selected by sharp-cut filters (Toshiba R62 and R63), and an interference filter (center wavelength: ~6600 Å, band pass: ~150 Å). The signal was recorded by a personal computer which controls also the laser wave number. In measurements of hole spectra, we irradiated a sample by the laser light with a fixed wavelength for the desired time. Then, we measured hole spectra with laser light attenuated by a factor of ~100 as luminescence excitation spectra by scanning the laser around the burning wave number. The scanning range was monitored by a Fabry-Perot-type spectrum analyzer.

III. RESULTS AND DISCUSSION

A. MgO-doping dependence of holes

Figure 1 shows persistent hole spectra burned at 20 K in five MgO-doped Y_2O_3:Pr^{3+} crystals. Burning laser intensity was 2 W/cm^2 and burning time was 60 s. We find clearly that the hole is deeper and broader as Y_2O_3:Pr^{3+} includes a larger amount of MgO. This result suggests that MgO doping induces the persistent hole.

These holes have no antihole and are not erased by 300 K annealing.[16,17] The possible formation mechanisms are local lattice rearrangement around Pr^{3+} ions, or photoionization from Pr^{3+} to Pr^{4+}. Photoionization phenomenon was recently observed in Pr^{3+}:YAG by using photon-gated photoconductivity,[25] but there is no example of photoionization hole burning in Pr^{3+}-doped materials. In addition, holes coming from photoionization need at least two photons of 6189 Å, considering $4f5d$ absorption bands for photoionization. It brings about quadratic or larger burning-intensity dependence of holes. However, in these Y_2O_3:Pr^{3+} systems, roughly linear dependence was observed between 2 W/cm^2 and 300 W/cm^2 burning. Therefore, the lattice rearrangement mechanism is more likely in these systems.[26]

In Fig. 2, hole widths [half width at half maximum (HWHM), MHz] are plotted against burning time. Samples are Y_2O_3:Pr^{3+} (asterisks), Y_2O_3:Pr^{3+}-Mg(0.1) (triangles), -Mg(0.3) (squares), -Mg(0.6) (circles), and -Mg(1) (crosses). At all the burning times, the width becomes larger as Y_2O_3:Pr^{3+} crystals include a larger amount of MgO. In each sample, we obtained a homogeneous linewidth (Γ_{hom}) from the zero-burning limit of the hole width (HWHM) from the

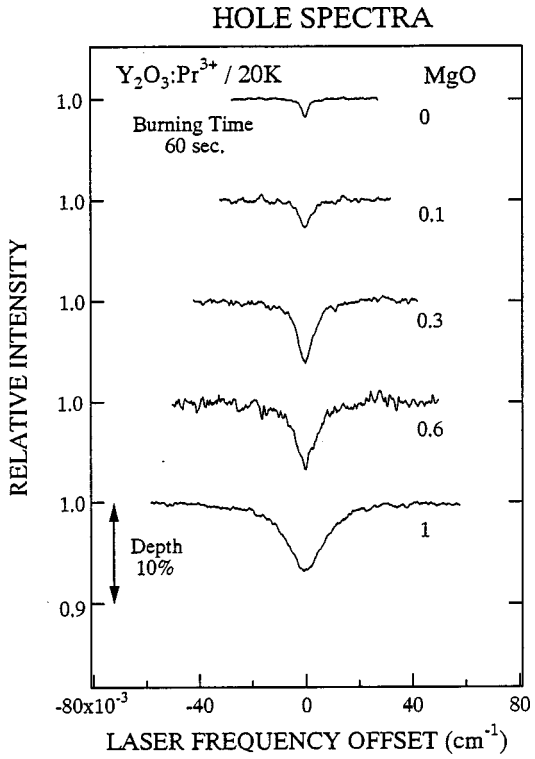

FIG. 1. Hole spectra at 20 K in $Y_2O_3:Pr^{3+}$, $Y_2O_3:Pr^{3+}$-Mg(0.1), -Mg(0.3), -Mg(0.6), and -Mg(1). Burning intensity is 2 W/cm^2 and burning time is 60 s.

data shown in Fig. 2. The obtained values are not far from the leftmost points corresponding to 5 s burning, which is practically zero burning on the time scale of this figure.

In Fig. 3, homogeneous linewidths are plotted against the concentration of MgO. We find that the linewidth shows

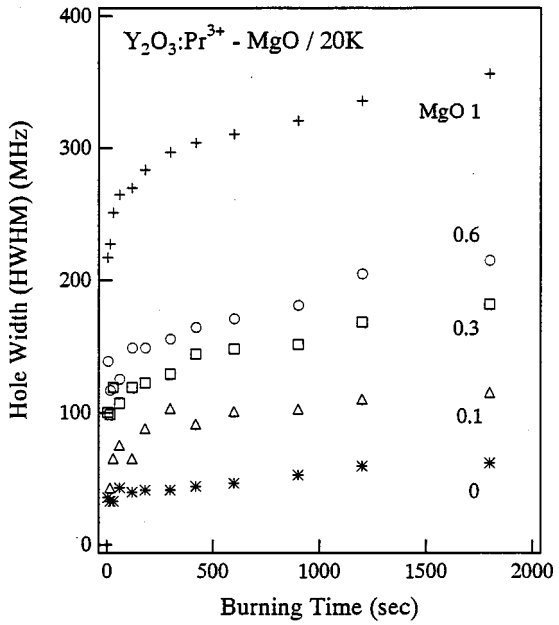

FIG. 2. Burning time dependence of hole width (half width at half maximum, HWHM) at 20 K in $Y_2O_3:Pr^{3+}$ (asterisks), $Y_2O_3:Pr^{3+}$-Mg(0.1) (triangles), -Mg(0.3) (squares), -Mg(0.6) (circles), and -Mg(1) (crosses).

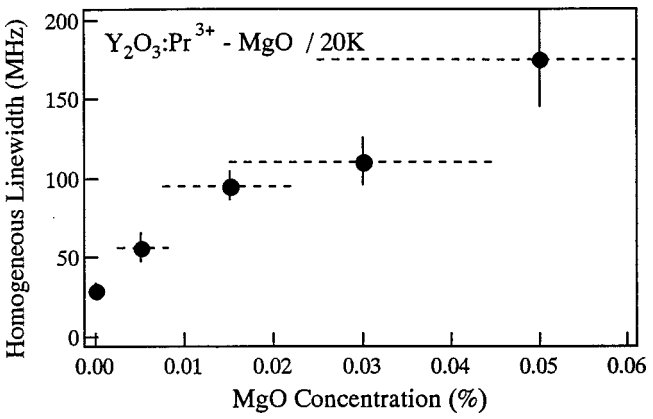

FIG. 3. MgO concentration dependence of homogeneous linewidth (Γ_{hom}) at 20 K in MgO-doped $Y_2O_3:Pr^{3+}$, determined from zero-burning limit of hole widths.

nearly linear dependence on the MgO concentration. This figure will be discussed in Sec. III D.

In order to compare the hole growth among the five samples, hole areas [depth (maximum 100%)×hole width (full width at half maximum (FWHM), MHz)] are plotted against burning time in log-linear scale in Fig. 4 (we confirmed that the product of the depth and the width is equal to the hole area within 10%). Samples and corresponding symbols are the same as those in Fig. 2.

We can assume that the oscillator strength of the $^3H_4$-$^1D_2$ transition of the optical centers (Pr^{3+}) is not changed among the five samples. Then the area of absorption spectrum is proportional to the number of the centers. This means that the hole area is proportional to the number of burned centers. This is fulfilled among the five samples with the different homogeneous linewidths.[27] Thus we can compare the hole-burning efficiency among the five samples by using hole areas shown in Fig. 4.

In Fig. 4, the area becomes larger as the burning time increases in all the samples, and the area is larger as a $Y_2O_3:Pr^{3+}$ crystal includes a larger amount of MgO at all the burning times.

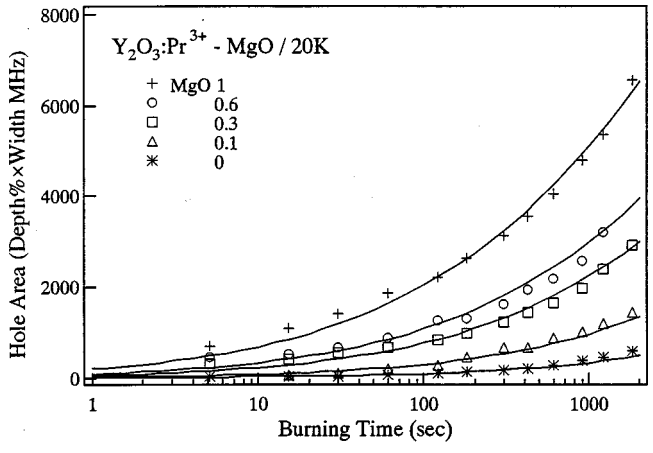

FIG. 4. Burning-time dependence of hole area [depth(%)×hole width (FWHM, MHz)] at 20 K in MgO-doped $Y_2O_3:Pr^{3+}$ plotted against logarithmic burning-time scale; the samples are $Y_2O_3:Pr^{3+}$ (asterisks), $Y_2O_3:Pr^{3+}$-Mg(0.1) (triangles), -Mg(0.3) (squares), -Mg(0.6) (circles), and -Mg(1) (crosses). Curves are the fitting results (see text).

B. Dispersive hole growth kinetics

1. Model

In the first place, we discuss a model to describe the burning curves shown in Fig. 4. We assume that depletion of the original centers and buildup of products by hole burning is governed by a rate constant K_t [$K_t=(k_t/k_f)qI$, where k_t is a tunneling rate to the photoproduct in the excited state, k_f is the relaxation rate from the excited state to the ground state (the reciprocal lifetime), q is the absorption cross section, and I is the photon flux].[28] The normalized concentration of the centers M is written by a rate equation

$$(d/dt)M(t)=-K_tM(t), \tag{1}$$

where $M(0)=1$. We assume that the optical centers couple to two-level systems (TLS) of the matrix, although these samples used in this research are crystalline. Even in crystals, a sample-dependent rather broad linewidth is found in Refs. 14, 29, 30. It was reported that Y_2O_3:Eu^{3+} fiber samples have low-energy states whose excitation energies, tunneling rates, and coupling strengths exhibit a broad distribution as in the case of glasses.[29,30] After optical excitation during the hole-burning process, tunneling occurs within the double-well potential coming from TLS with a rate constant K_t. We assume that the burning rate K_t is given by $K_t=K_t^0\exp(-\lambda)$, where λ is the tunneling parameter of the general form $(2mVd^2/h^2)^{1/2}$ (m is the mass of the tunneling entity, V is the barrier height, and d is the width of the barrier),[28,31–33] and K_t^0 is an attempt frequency on the order of an optical-phonon frequency.[28] After the tunneling occurs and the optical center relaxes to the electronic ground state, absorption frequency of the center changes, and then a hole is produced.[34]

If the rate K_t is common to all the centers, hole-growth data should follow a simple exponential of $M(t)=\exp(-K_tt)$ from Eq. (1). Nevertheless, all of the data in Fig. 4 do not follow a simple exponential profile; the time development of the hole area largely deviates from an exponential function and shows saturationlike behavior at longer burning times. The simple optical saturation effect cannot explain these nonexponential profiles, because the maximum hole depth is less than 20% in the experiments here. In some cases, such profiles in hole-burning kinetics could be explained by introducing distribution into λ. Then, $M(t)$ can be written as

$$M(t)=\int g(\lambda)\exp[-K_t^0\exp(-\lambda)]d\lambda,$$

where $g(\lambda)$ is a distribution function of λ and $\int g(\lambda)d\lambda=1$. The introduction of distribution into K_t^0 seems unnecessary, because the fluctuation of the factor $\exp(-\lambda)$ would give far larger effect.[35,28] This distribution of λ may include its variation in one sample between the centers just resonant with the laser and those absorbing the laser at the wing of their homogeneous linewidths. Some reports used flat distribution for λ with cutoff procedure.[36,37] Others used Gaussian distribution.[38,39]

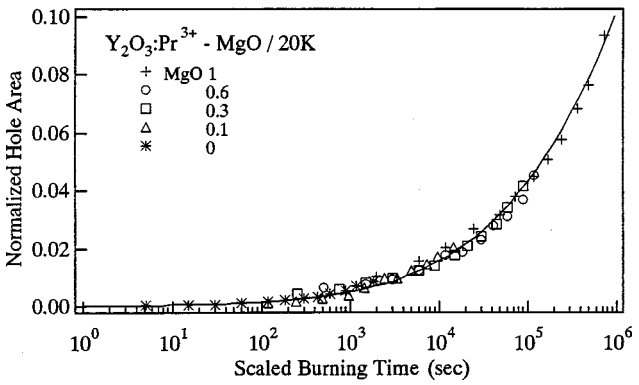

FIG. 5. Relative hole area plotted against scaled burning time (see text for the scaling) at 20 K in MgO-doped Y_2O_3:Pr^{3+} plotted in log-linear scale; the samples are Y_2O_3:Pr^{3+} (asterisks), Y_2O_3:Pr^{3+}-Mg(0.1) (triangles), -Mg(0.3) (squares), -Mg(0.6) (circles), and -Mg(1) (crosses). The curve shows calculation based on a model in the text.

2. Scaling of the data among the samples

Before trying to fit the hole-growth data in Fig. 4, we examine the possibility of scaling of the hole-growth data. Among the five samples used here, we changed only the concentration of MgO. Hence we might expect that the data in the samples follow a simple scaling law. There are two ways of scaling, that is, the scaling of the ordinate, and that of the abscissa. Hole-growth data of Pr^{3+} ions in germanate glasses were well explained by the former scaling.[40] Nevertheless, we find that the data in these MgO-doped Y_2O_3:Pr^{3+} crystals do not follow a single curve only by multiplication by each factor in the ordinate scale [for example, the asterisk (Y_2O_3:Pr^{3+}) at 2000 s is located at $\sim$1/10 of the cross, Y_2O_3:Pr^{3+}-Mg(1), at 2000 s, while the asterisk at 5 s is at $\sim$1/40 of the cross]. Thus, the scaling of the ordinate cannot be applied to these data.

Then we apply the scaling of the burning time (the abscissa). For this scaling, we use the data in Fig. 4 and assume the appropriate scaling factor for burning time (burning rate) in each sample. By using each normalized time (each burning rate) for each sample, we plot hole areas in the five samples in Fig. 5 (the ordinate of this figure is divided by 70 000 from Fig. 4, which will be explained in the fitting procedure). Samples and corresponding symbols are the same as those for Fig. 2. We find that all of the data reasonably follow a single curve in the figure (a theoretical fit in the next subsection), that is, the hole-growth data in these MgO-doped samples follow the scaling of the burning time. The ratio of the normalization factor for burning time is (1:8:50:100:400) for Y_2O_3:Pr^{3+}, Y_2O_3:Pr^{3+}-Mg(0.1), -Mg(0.3), -Mg(0.6), and -Mg(1).

The application of this scaling means that only the average burning efficiency of Pr^{3+} ions is different among the five samples. Nonexponential hole-growth curves suggested the dispersion in the burning rate K_t (or λ) as is mentioned above. The existence of the scaling law in the burning time indicates that there is no difference in the dispersion in the burning rate.

3. Fitting the data

The next step is to fit the hole areas in all of the burning times, that is, to find a good distribution function of $g(\lambda)$

explaining the whole hole-growth curve in Fig. 5. At first, we consider the flat distribution for λ, which was successfully applied to R' color centers in LiF crystals.[41] It brings a logarithmic time dependence of the hole area, that is, a straight hole-growth line against burning time in log-linear scale. As is found in Fig. 4, it cannot be applied to these results.

Next, we try to use Gaussian distribution for $g(\lambda)$,[28] that is,

$$g(\lambda)=\sqrt{\frac{2}{\pi\sigma^2}}\exp\left(-\frac{(\lambda-\lambda_0)^2}{2\sigma^2}\right),$$

where λ_0 is the center of the distribution of λ, and σ is the width of the Gaussian. Then, we can write the expression for $M(t)$ as

$$M(t)=\sqrt{\frac{2}{\pi\sigma^2}}\int_{-\infty}^{\infty}\exp\left[-\frac{(\Delta\lambda)^2}{2\sigma^2}-K_t^0 t \times\exp\{-(\lambda_0+\Delta\lambda)\}\right]d(\Delta\lambda), \quad (2)$$

where $\Delta\lambda=\lambda-\lambda_0$ (deviation of the tunneling parameter).

Before we apply the Gaussian distribution, we normalize the hole area in Fig. 4. We consider the maximum number of centers which can possibly be burned. Then, we use 70 000 $=2$ (broadening)$\times$175 MHz [homogeneous width of the broadest sample, Y_2O_3:Pr^{3+}-Mg(1)]$\times 2$ (full width)$\times$100% (full depth) for the normalization factor. This was used in the ordinate of Fig. 5. In Fig. 2, the maximum hole width is about twice that of the homogeneous width, thus we use the factor 2 as the effect of broadening. The maximum homogeneous width is used among the five samples. It is not clear that a hole with such a large area of 70 000 can be really burned even in Y_2O_3:Pr^{3+} with the smallest homogeneous linewidth. Nevertheless, the burning rate can be compared by fair means using hole areas among the five samples regardless of the normalization factor, as is described in Sec. III A. In addition, centers impossible to be burned can be regarded as those hardly burned in the wing of the Gaussian distribution of the burning rate. Therefore, we assume this normalization factor.

Here, we try to fit the shape of the universal curve in Fig. 5 by using the two fitting parameters of σ and K [$K\equiv K_t^0\exp(-\lambda_0)$]. The result of fitting is shown in Fig. 5 by the solid curve, where σ and K are determined to be 5 and $7.6\times10^{-10}\,s^{-1}$, respectively. The used parameter for the abscissa for each sample is $K\times$ (burning time)$\times 1$, 8, 50, 100, or 400 for Y_2O_3:Pr^{3+}, Y_2O_3:Pr^{3+}-Mg(0.1), -Mg(0.3), -Mg(0.6), or -Mg(1), respectively, and the calculated results are shown in Fig. 4 by lines. These five values for the five kinds of MgO-doped samples mean the relative hole-burning rate, and correspond to the normalization factor obtained in the scaling procedure from Fig. 4 to Fig. 5 at the end of the preceding subsection. The agreement between the data and the calculation in Figs. 4 and 5 is satisfactory.

4. Meaning of the model

We consider the meaning of this model and the parameter K. When we introduce the distribution into λ, the rate of the depletion of centers $K_t^0\exp(-\lambda)$ begins to have distribution. It means that there are centers which can easily be burned and those which can hardly be burned. The area of a hole in a spectrum is proportional to the number of burned centers. Thus, some small hole can be burned in a very short burning time, while a very long time is necessary to burn a large hole. Figure 6 shows calculated results for distribution of remaining centers in the kinetic experiments when the time proceeds.[28] In this figure, the integrand in Eq. (2) using $\sigma=5$ for several values of normalized burning time t is plotted against the deviation of the tunneling parameter $\Delta\lambda$. The curve denoted by $t=0$ shows the distribution of λ for the centers before burning. In the experiment of Fig. 4, normalized burning time ranges from 5 to $\sim10^6$ which depends both on time and the samples. We find that only the centers which can easily be burned in the tail of the distribution of λ contribute to the hole in this experiment.

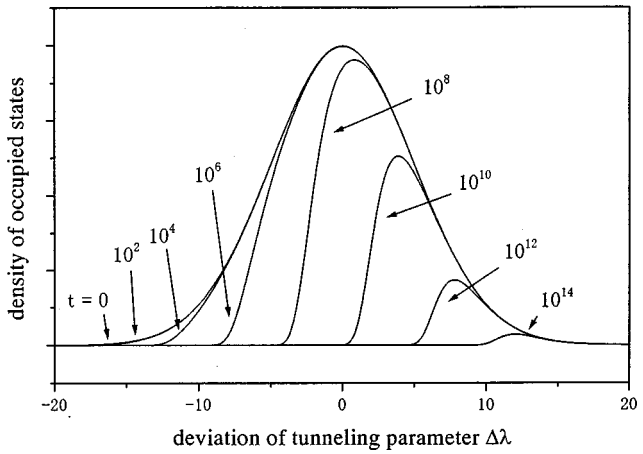

FIG. 6. Time evolution of density of original centers against the deviation of tunneling parameter ($\Delta\lambda=\lambda-\lambda_0$). Values of t indicate burning times.

In Fig. 7, the scaling factor of burning time, that is, the relative burning rate, is plotted against the concentration of MgO in the five kinds of Y_2O_3:Pr^{3+}-Mg samples. We find that the factor shows an increase with the increase of the MgO concentration. This figure will be discussed in Sec. III D.

C. Effect of other metallic ion doping

In addition to the MgO-doped samples, we investigated Y_2O_3:Pr^{3+} samples doped with various other metal oxides,

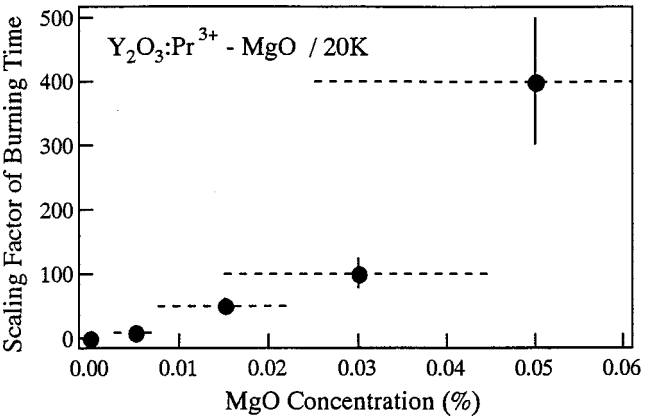

FIG. 7. MgO-concentration dependence of scaling factor of burning time or relative burning rate at 20 K determined from fitting of the hole-growth data in Fig. 5.

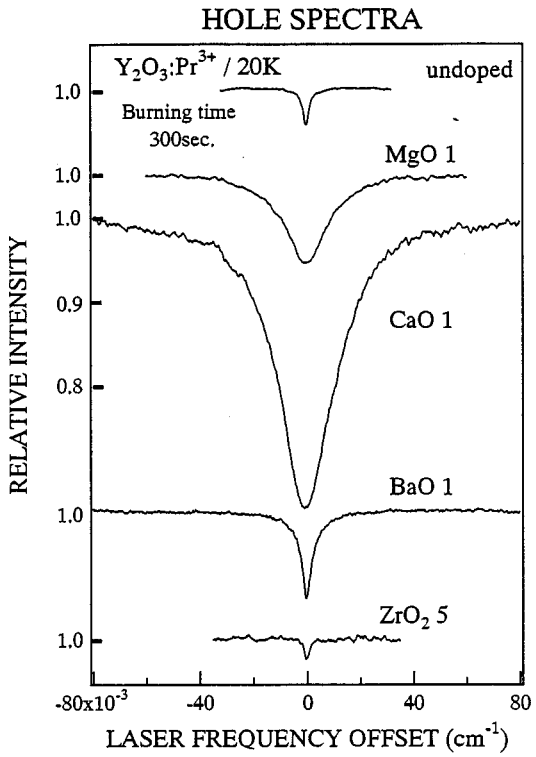

FIG. 8. Hole spectra at 20 K in five Y_2O_3:Pr^{3+} crystals doped with other metallic ions [Y_2O_3:Pr^{3+} (undoped), Y_2O_3:Pr^{3+}-Mg(1), -Ca(1), -Ba(1), and -Zr(5)]. Burning intensity is 2 W/cm^2 and burning time is 300 s.

that is, Y_2O_3:Pr^{3+}-Ca(1), -Ba(1), and -Zr(5) in Table I. Figure 8 shows hole spectra burned at the same burning condition (2 W/cm^2×300 s) at 20 K in Y_2O_3:Pr^{3+} (undoped), Y_2O_3:Pr^{3+}-Mg(1), -Ca(1), -Ba(1), and -Zr(5).

We find that the holes in Y_2O_3:Pr^{3+} (undoped) and Y_2O_3:Pr^{3+}-Zr(5) have almost the same width and area. This fact suggests that the Zr^{4+} doping does not affect hole properties in Y_2O_3:Pr^{3+} crystals. On the other hand, when any kind of M^{2+} (M^{2+}:Mg^{2+}, Ca^{2+}, or Ba^{2+}, that is, divalent metallic ion) is included in the crystals, the observed hole width and area become larger than those in the undoped crystal; we will discuss the difference of the width and the area among the three M^{2+}-doped samples in the next section.

Considering charge compensation in the doping of divalent ions into Y_2O_3:Pr^{3+} crystals, we can expect that the introduction of M^{2+} into the Y^{3+} site is accompanied by oxygen vacancies (one vacancy for two M^{2+} ions). On the other hand, in Zr^{4+}-doped Y_2O_3:Pr^{3+}, no oxygen vacancy is produced; interstitial oxygen ions or metallic ion vacancies should be produced. From this consideration, it is thought that the oxygen vacancies play an important role in the hole broadening and the production of persistent holes.

D. Role of oxygen vacancies in hole properties

The determination of the precise origins of the hole broadening and the hole production might be difficult. We presume that the oxygen vacancies are at least one of the origins. It is possible that other defects introduced with M^{2+}-doping may also be important. However, the characterization of such defects and the estimation of their densities are quite difficult here. In this section, we discuss the charge-compensating oxygen vacancies as entities contributing to the hole broadening and the hole production.[42]

One of the important unsolved problems about hole-burning or linewidth related to TLS is whether they are induced by a TLS adjacent to the center, or by a lot of TLS spread over the matrix.[4] This is, in other words, the problem of the interaction length between the center and the TLS. When it is long, a center will be affected by many TLS distributed uniformly in a host. On the other hand, when the interaction length is short, a center will be influenced only by a small number of TLS surrounding the center, or even by one TLS adjacent to the center.

The nature of TLS contributing to hole production and that to hole broadening might be different. The TLS which produces a persistent hole should flip in the time scale of the hole formation (seconds to hours), while TLS which broadens linewidth should flip in the time scale of the reciprocal of the linewidth (ns to μs). However, it has been shown in the above discussions that both types of TLS is introduced simultaneously, accompanying the oxygen vacancies. Therefore, in the following, we discuss hole production and hole broadening in the same way.

1. Interaction length between Pr^{3+} ions and oxygen vacancies

Firstly, we examine the spatial distribution of oxygen vacancies; whether the vacancies are distributed uniformly in the crystals, or gather around Pr^{3+} ions. For this purpose, we made hole-burning experiments on the sample with the initial concentration in the starting mixtures of (Y_2O_3)(99.89 mol %)-Pr_2O_3(0.01 mol %)-MgO(0.1 mol %); it has one order of magnitude lower concentration of Pr^{3+} (0.02 mol %) than other samples. Considering the reduction factor 1/20 for Mg^{2+} in sample growing obtained in Sec. II, real concentration of Mg^{2+} is 0.005 mol % (see Table I and the uncertainty is ~50%). In Fig. 9, we compare hole spectra at 20 K in (a) Y_2O_3:Pr^{3+}(0.02)-Mg(0.1), (b) :Pr^{3+}(0.2)-Mg(0.1), and (c) :Pr^{3+}(0.2)-Mg(1). The burning intensity is 2 W/cm^2 and the burning time is 15 s.

If the interaction length is short and the oxygen vacancies tend to gather around Pr^{3+} ions, the results of (a) and (c) should be similar; it is because the ratio of MgO to Pr^{3+} is the same and thus each Pr^{3+} ion in both the samples feels about the same effect of the same number of vacancies. However, the result is significantly different. The hole in (c) is far larger than that in (a). On the other hand, when the interaction length is long and the oxygen vacancies are distributed uniformly, the results of (a) and (b) should be similar; it is because the concentration of MgO is the same and thus each Pr^{3+} ion feels the same effect of the vacancies irrelevant to the concentration of Pr^{3+}. Since the hole in (a) is close to that in (b), we find that the latter situation is more likely. This situation was the same for other burning times. Therefore, we can presume that a Pr^{3+} ion interacts in a long distance with oxygen vacancies distributed uniformly in the host crystal.

Secondly, we estimate the density of the oxygen vacancies and Pr^{3+} ions. In the Y_2O_3:Pr^{3+}(0.2 mol %) crystals, the number density of Pr^{3+} ions on the C_2 site is calculated to be 2×10^{19} cm^{-3}, using a lattice constant 10.6 Å.[43] Here we

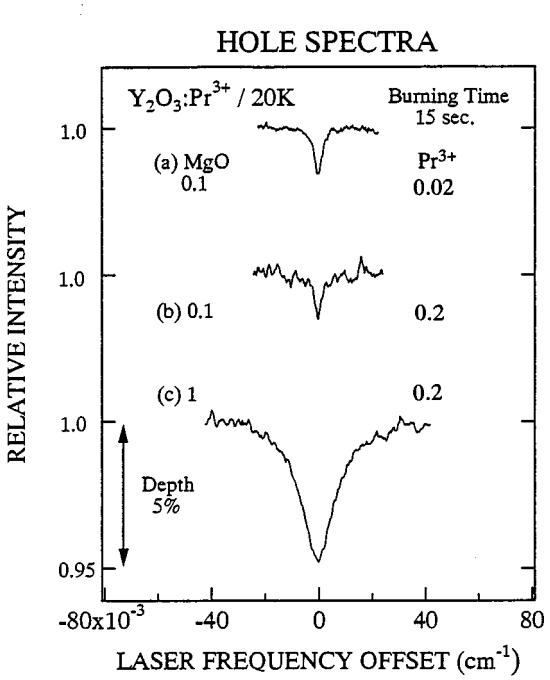

FIG. 9. Hole spectra at 20 K in three kinds of MgO-doped Y_2O_3:Pr^{3+} [(a) Y_2O_3:Pr^{3+}(0.02)-Mg(0.1), (b) Y_2O_3:Pr^{3+}(0.2)-Mg(0.1), and (c) Y_2O_3:Pr^{3+}(0.2)-Mg(1)]. Burning intensity is 2 W/cm^2 and burning time is 15 s.

assumed 3/4 of the doped Pr^{3+} ions are substituted to the C_2 site. The density of the oxygen vacancies in Y_2O_3:Pr^{3+}(0.2)-Mg(0.1), for example, is estimated to be 1/30 of the Pr^{3+} ions, that is, $6.7\times10^{17}\,\mathrm{cm}^{-3}$ (uncertainty $\sim$50%), considering the reduction factor of 1/20 for Mg^{2+} in sample growing.

This small ratio 1/30 confirms the uniformly distributed oxygen vacancies as follows. If an oxygen vacancy tends to be located near a Pr^{3+} ion and the Pr^{3+} ion interacts only with the neighboring vacancy, at least 29/30 of Pr^{3+} ions could not interact with oxygen vacancies in Y_2O_3:Pr^{3+}(0.2)-Mg(0.1). Then the hole production and broadening would be induced only in 1/30 of Pr^{3+} ions and not in 29/30. In this case, we can expect almost no change in the hole behavior of Y_2O_3:Pr^{3+}(0.2)-Mg(0.1), comparing it with undoped Y_2O_3:Pr^{3+}. Nevertheless, this is not the case for the results in Sec. III A, because the homogeneous linewidth or the average burning rate is about twice or eight times as large as those in undoped Y_2O_3:Pr^{3+} in Figs. 3 or 7. Therefore, it is most probable that the interaction between oxygen vacancies and Pr^{3+} ions is not a local one but extends to a long distance, that is, the Pr^{3+} ions feel the vacancies in a rather large volume which contains several or more vacancies.

From the above discussions, we found that even quite a small number of oxygen vacancies, that is, 1/30 of the number of Pr^{3+} ions [in Y_2O_3:Pr^{3+}(0.2)-Mg(0.1)], can affect both the hole-burning rate and the width in almost all the Pr^{3+} ions in the sample. Because the number of the Pr^{3+} ions is far larger than that of the vacancies, we can estimate the lower limit of interaction length between oxygen vacancies and Pr^{3+} ions as half of the average distance between oxygen vacancies in this sample. This length is approximately calculated as $(6.7\times10^{17}\,\mathrm{cm}^{-3})^{-1/3}/2=\sim60$ Å (uncertainty $\sim$20%).

When a larger amount of the vacancies are introduced into the crystal, the number of the vacancies felt by one Pr^{3+} ion increases. When we assume that the homogeneous linewidth is in proportion to the number of the vacancies affecting a Pr^{3+} ion, the linewidth becomes larger with the increase of the vacancies. In the same way, when we assume that the average burning rate is in proportion to the number of the vacancies affecting a Pr^{3+} ion, the rate becomes larger with the increase of the vacancies. From these assumptions, we can understand qualitatively the roughly linear relations between the linewidth and the concentration of MgO shown in Fig. 3, and between the burning rate and the MgO concentration in Fig. 7.

In Figs. 3 and 7, the linewidth and the burning rate seem to have different MgO concentration dependence; the homogeneous linewidth (the burning rate) may have weaker (stronger) dependence than the linear dependence on MgO concentration. This may reflect the different nature of TLS contributing to hole broadening or to hole production. However, we do not discuss their discrimination, because the present results do not have enough data points or accuracy for such a discussion.

In the discussion above, we presumed the long-range interaction between Pr^{3+} ions and oxygen vacancies, and we estimated the lower limit of the interaction length as $\sim$60 Å. If the interaction length is large enough, hole-burning dynamics of the irradiated ensemble of ions might be describable by a single average response. This was not the case and the dispersive hole-growth kinetics was obtained, as was found in Sec. III B. Thus there should be the upper limit of the interaction length. Obtaining the upper limit or the precise length is left as a future problem.

The Y_2O_3 structure can be thought of as a defective CaF_2 structure, where the metallic ions are distributed on the calcium sites but the oxygen ions occupy only three-fourths of the fluorine positions.[23] As was mentioned before,[19] this structure with one-fourth of the anion sites vacant seems susceptible for defects on the oxygen sublattice. It might be possible that one extra oxygen vacancy introduced by M^{2+} doping induces disordered oxygen arrangement on the sublattice. For example, if one oxygen vacancy is introduced, the surrounding anion vacant sites will be rearranged and thus the disorder might extend to more than several unit cells. We did not consider such an effect in the above discussion, and assumed that charge-compensating oxygen vacancies do not exchange any other vacancies and oxygen ions. When we include this effect, the length of $\sim$60 Å obtained above can be regarded as the lower limit of the distance in which the disorder is brought about by the charge-compensating oxygen vacancy. If we follow this assumption, the cause of hole burning might somewhat be the short-range interaction between the center and this disorder. Then, this short-range interaction seems likely to induce dispersive hole-growth kinetics in Fig. 6, as is described in the preceding paragraph. In any case, the length in which the effect of the oxygen vacancy on hole burning extends is obtained to be larger than $\sim$60 Å.

We consider other unknown defects as the origin of the hole burning instead of oxygen vacancies, as was mentioned in Sec. III D. The similar rough estimation might be possible for the defects which would be introduced with M^{2+} doping.

Because the density of M^{2+} ions is twice that of oxygen vacancies, the lower limit in which the defects are brought about or the effect of the defect extends, is estimated to be $[(\sim 60\,\text{Å})^3/2]^{1/3} = \sim 50\,\text{Å}$ (uncertainty ~20%). However, the characterization of the defects may be needed, in order to make such discussion more reliable.

2. Comparing holes in Y_2O_3:Pr^{3+}-Mg(1), -Ca(1), and -Ba(1)

In this subsection, we discuss hole width and hole-burning efficiency in the samples with the three different kinds of divalent ions shown in Fig. 8 [Y_2O_3:Pr^{3+}-Mg(1), -Ca(1), and -Ba(1)]. From the results in Table I, the divalent ion concentration in Y_2O_3:Pr^{3+}-Ca(1) is the largest and that in -Ba(1) is the smallest. This order of concentration is supported by the inhomogeneous linewidths shown in Table I. The width is the largest in -Ca(1) and the smallest in -Ba(1).

In Fig. 8, we can compare areas and widths of the holes burned in the three M^{2+}-doped samples in the same condition at 20 K. We find that the order of the area and the width is the same as that of the concentration of M^{2+}; they are the largest in Y_2O_3:Pr^{3+}-Ca(1) and the smallest in -Ba(1).

These results show that holes are broader and are more easily burned as a Y_2O_3:Pr^{3+} crystal includes a larger amount of M^{2+} ions irrelevant to the kind of M^{2+}. This fact supports our conclusion that the hole-burning efficiency and the hole width are controlled by the concentration of oxygen vacancies, not by the doped metallic ions directly.

E. Temperature dependence of homogeneous linewidth in Y_2O_3:Pr^{3+}, Y_2O_3:Pr^{3+}-Mg(0.1), and -Mg(1)

We measured homogeneous linewidth (Γ_{hom}) in Y_2O_3:Pr^{3+}-Mg(0.1) and -Mg(1) at various temperatures. In Fig. 10 the results are plotted; closed squares and circles are the results of Y_2O_3:Pr^{3+}-Mg(0.1) and -Mg(1), respectively. Triangles are the results of undoped Y_2O_3:Pr^{3+} and crosses are of Y_2O_3:Pr^{3+} grown in an air atmosphere.[14]

In the MgO-doped samples, we obtained Γ_{hom} between 230 and 119 K from luminescence spectra under nonselective excitation using a xenon lamp with a broad bandpass filter, as the homogeneous linewidth is larger than the inhomogeneous linewidth at high temperatures. In this temperature region, the linewidth in these three samples shows about the same value. Below 40 K, Γ_{hom} was determined from the hole-burning experiment (the zero-burning limit of the half width at half maximum of holes). Below 9 K, it was difficult to determine Γ_{hom} (zero-burning limit) for the doped samples in the present setup, because holes burned at this temperature contain the hole component due to the optical pumping with short lifetime.[17,20] The linewidth in undoped Y_2O_3:Pr^{3+} between 60 and 30 K (open triangles) was obtained from fluorescence-line-narrowing technique, and that at 20 and 10 K (closed triangles) was from hole-burning measurement.[14] Bars in the figure show the typical error ranges.

In undoped Y_2O_3:Pr^{3+}, the temperature dependence of the homogeneous linewidth down to 30 K follows the Raman process curve which is shown by a dashed line in the figure.[14] However, in the MgO-doped samples the linewidth begins to deviate from the dashed line around 30 K. At lower temperatures, the linewidth shows the *T*-linear-like (*T*: temperature) dependence similar to that observed in the air-grown Y_2O_3:Pr^{3+} (crosses). This behavior, i.e., weak temperature dependence of linewidth at low temperature, is similar to the linewidth in other disordered materials such as yttria-stabilized zirconia or silicate glass.[44,13,14,18] By comparing these two kinds of MgO-doped samples, we find that the linewidth becomes larger as a Y_2O_3:Pr^{3+} crystal includes larger amount of MgO at all the temperatures below 20 K.

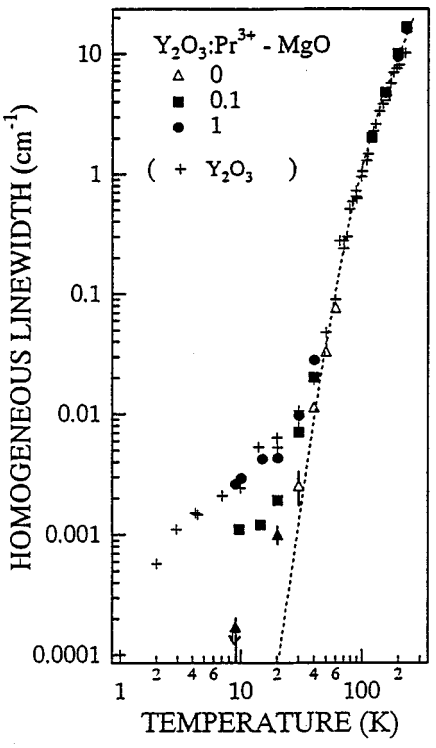

FIG. 10. Temperature dependence of homogeneous linewidth plotted in log-log scale in MgO-doped Y_2O_3:Pr^{3+} crystals; the samples are Y_2O_3:Pr^{3+} (triangles), Y_2O_3:Pr^{3+}-Mg(0.1) (squares), and -Mg(1) (circles). The linewidth between 230 and 120 K was obtained from luminescence linewidth in the three samples, and all of them show approximately the same linewidth; the corresponding symbols are superposed each other. The linewidth in the two MgO-doped samples between 40 and 10 K (squares and circles) was obtained from hole-burning measurement. The linewidth in Y_2O_3:Pr^{3+} between 60 and 30 K (open triangles) was obtained from fluorescence-line-narrowing technique, and that at 20 and 10 K (closed triangles) was from hole-burning measurement (Ref. 14). Cross symbols denoting linewidth in Y_2O_3:Pr^{3+} grown in an air atmosphere, and dashed curve indicating a theoretical fit of the Raman process were also described in Ref. 14.

IV. SUMMARY

In this paper, we investigated holes due to the local lattice rearrangement in metallic ion-doped Y_2O_3:Pr^{3+} crystals under the systematic control of disorder. In MgO-doped samples, we found that hole width (homogeneous linewidth) is larger as the concentration of MgO increases. In the analysis of hole-growth data in the MgO-doped samples, they follow the scaling of the burning time. This scaled growing profile was successfully fitted by assuming that all Pr^{3+} ions are coupled to many two-level systems and that the tunneling parameter has the Gaussian distribution. We found that the burning rate increases monotonically with the increase of the concentration of MgO.

When we compare the results of other metallic ion doping, we find that divalent ion induces hole broadening and hole production while Zr^{4+} ion does not. Hence, oxygen vacancies introduced into the crystals by divalent-ion doping is probably one of the origins of the line broadening and the hole production.

From the relation between the hole-burning data and the concentration of oxygen vacancies, a Pr^{3+} ion is considered to interact with oxygen vacancies distributed uniformly in the host crystal with an interaction length larger than ~60 Å (uncertainty ~20%).

As for the temperature dependence of homogeneous linewidth, the MgO-doped samples show *T*-linear-like behavior below ~30 K. The effect of disorder concerned with oxygen vacancies on linewidth is thought to be revealed in this low-temperature region.

*Present address: Institute of Physics, University of Tsukuba, Tsukuba, Ibaraki 305-8571, Japan.

[1] W. A. Phillips, Rep. Prog. Phys. **50**, 1657 (1987).
[2] Clare C. Yu and A. J. Leggett, Comments Condens. Matter Phys. **14**, 231 (1988).
[3] D. A. van de Straat, J. Baak, H. B. Brom, Th. Schmidt, and S. Völker, Phys. Rev. B **53**, 2179 (1996).
[4] *Persistent Spectral Hole-Burning: Science and Applications*, edited by W. E. Moerner (Springer-Verlag, Berlin, 1988).
[5] R. Jaaniso and H. Bill, Europhys. Lett. **16**, 569 (1991).
[6] K. Holliday, C. Wei, M. Croci, and U. P. Wild, J. Lumin. **53**, 227 (1992).
[7] K. Hirao, J. Non-Cryst. Solids **196**, 16 (1996).
[8] K. Koyama and T. Suemoto, J. Lumin. **66&67**, 164 (1996).
[9] H. Yugami, R. Yagi, S. Matsuo, and M. Ishigame, Phys. Rev. B **53**, 8283 (1996).
[10] R. M. Macfarlane, R. J. Reeves, and G. D. Jones, Opt. Lett. **12**, 660 (1987).
[11] R. J. Reeves and R. M. Macfarlane, J. Opt. Soc. Am. B **9**, 763 (1992).
[12] S. Matsuo, H. Yugami, M. Ishigame, and S. Shin, J. Lumin. **64**, 267 (1995).
[13] K. Tanaka, T. Okuno, H. Yugami, M. Ishigame, and T. Suemoto, Opt. Commun. **86**, 45 (1991).
[14] T. Okuno, K. Tanaka, K. Koyama, M. Namiki, and T. Suemoto, J. Lumin. **58**, 184 (1994).
[15] T. Suemoto, T. Okuno, and D. Nakano, Opt. Commun. **145**, 113 (1998).
[16] T. Okuno, K. Tanaka, and T. Suemoto, Opt. Commun. **123**, 512 (1996).
[17] T. Okuno and T. Suemoto, J. Lumin. **66&67**, 179 (1996).
[18] Th. Schmidt, R. M. Macfarlane, and S. Völker, Phys. Rev. B **50**, 15 707 (1994).
[19] K. W. Jang and R. S. Meltzer, Phys. Rev. B **52**, 6431 (1995).
[20] T. Okuno, K. Tanaka, and T. Suemoto (unpublished).
[21] H. Tuiki, K. Kitazawa, T. Masamoto, K. Shiroki, and K. Fueki, J. Cryst. Growth **49**, 71 (1980).
[22] From the several results of the analysis by using a few pieces, we found that Mg^{2+} ions tend to segregate in the macroscopic defects (analyzed pieces sometimes had lower quality than those used in the hole-burning experiments). On the other hand, the results of the hole burning was not influenced by Mg^{2+} in such positions. Therefore, this analysis is thought to show somewhat the higher limit of that concentration which we want to know. In Table I, *relatively* reliable values are shown.
[23] Ralph W. G. Wyckoff, *Crystal Structure*, 2nd ed. (Interscience, New York, 1960), Vol. 2, p. 3.
[24] R. P. Leavitt, J. B. Gruber, N. C. Chang, and C. A. Morrison, J. Chem. Phys. **76**, 4775 (1982).
[25] G. Wittmann and R. M. Macfarlane, Opt. Lett. **21**, 426 (1996).
[26] We assume the lattice rearrangement mechanism throughout the present paper. In Refs. 34 and 42, we mention the interpretation, when the hole formation mechanism is photoionization. The whole discussion in this paper holds for holes from photoionization.
[27] Assuming a constant oscillator strength and a very narrow bandwidth of the excitation light, the absorption probability is in inverse proportion to the homogeneous linewidth and the number of optical centers excited is in proportion to the homogeneous linewidth. Therefore, hole-burning velocity is not affected by the homogeneous linewidth, so long as we evaluate the velocity by increase of hole area per unit time. Thus we can compare the hole-burning efficiency among different samples with different homogeneous linewidths.
[28] R. Jankowiak, R. Richert, and H. Bassler, J. Phys. Chem. **89**, 4569 (1985).
[29] G. P. Flinn, K. W. Jang, Joseph Ganem, M. L. Jones, R. S. Meltzer, and R. M. Macfarlane, Phys. Rev. B **49**, 5821 (1994).
[30] M. J. Sellars, R. S. Meltzer, P. T. H. Fisk, and N. B. Manson, J. Opt. Soc. Am. B **11**, 1468 (1994).
[31] R. Jankowiak, L. Shu, M. J. Kenny, and G. J. Small, J. Lumin. **36**, 293 (1987).
[32] S. P. Love and A. J. Sievers, Chem. Phys. Lett. **153**, 379 (1988).
[33] S. P. Love, C. E. Murgan, and A. J. Sievers, J. Opt. Soc. Am. B **9**, 794 (1992).
[34] When we assume that the formation mechanism of this hole is photoionization from Pr^{3+} to Pr^{4+}, the electron separating from Pr^{3+} tunnels into some trap. The rate of this tunneling can be regarded as K_t.
[35] R. Richert, Chem. Phys. Lett. **118**, 534 (1985).
[36] P. Reineker, H. Morawitz, and K. Kassner, Phys. Rev. B **29**, 4546 (1984).
[37] S. Hunklinger and M. Schmidt, Z. Phys. B **54**, 93 (1984).
[38] R. Richert, B. Ries, and H. Bassler, Philos. Mag. B **49**, L25 (1984).
[39] R. Richert and H. Bassler, Chem. Phys. Lett. **116**, 302 (1985).
[40] T. Suemoto, M. Namiki, and K. Koyama, Opt. Commun. **115**, 475 (1995).
[41] W. M. Moerner, P. Pokrowsky, F. M. Schellenberg, and G. C. Bjorklund, Phys. Rev. B **33**, 5702 (1986).
[42] In the photoionization mechanism, an oxygen vacancy can be regarded as a trap of an electron separating from Pr^{3+}.
[43] A. A. Kaminskii, *Laser Crystals* (Springer, Berlin, 1981), p. 322.
[44] R. M. Macfarlane and R. M. Shelby, Opt. Commun. **45**, 46 (1983).